Chinese Chemical Letters 35 (2024) 108701

Contents lists available at ScienceDirect

Chinese Chemical Letters

journal homepage: www.elsevier.com/locate/cclet

A novel insight of enhancing the hydrogen peroxide tolerance of unspecific peroxygenase from *Daldinia caldariorum* based on structure

Tiantian Li[a], Ruochen Jin[a], Bin Wu[b], Dongming Lan[a], Yunjian Ma[a,*], Yonghua Wang[a,c,*]

[a] School of Food Science and Engineering, South China University of Technology, Guangzhou 510640, China
[b] School of Bioscience and Bioengineering, South China University of Technology, Guangzhou 510006, China
[c] Guangdong Youmei Institute of Intelligent Bio-manufacturing Co., Ltd., Foshan 528200, China

ARTICLE INFO

Article history:
Received 3 May 2023
Revised 12 June 2023
Accepted 15 June 2023
Available online 22 June 2023

Keywords:
Unspecific peroxygenase
Molecular modification
Hydrogen peroxide stability
Crystal structure
Hydroxyl fatty acids

ABSTRACT

Unspecific peroxygenases (UPOs, EC 1.11.2.1) is a kind of thioheme enzyme capable of catalyzing various oxidations of inert C–H bonds using H_2O_2 as an oxygen donor without cofactors. However, the enhancement of the H_2O_2 tolerance of UPOs is always challenging. In this study, the A161C mutant of *rDca*UPO, which originates from *Daldinia caldariorum*, was found to be highly H_2O_2-resistant. Compared with the wild type, the mutant *rDca*UPO-A161C showed a 10-h prolonged half-life and a 64% improved enzyme activity when incubated in 10 mmol/L H_2O_2. The crystal structure analysis at 1.47 Å showed that *rDca*UPO-A161C exhibited 10 α-helixes (cyan) and a series of ordered rings, forming a single asymmetric spherical structure. The two conserved domains near heme formed an active site with the catalytic PCP and EHD regions (Glu86, His87, Asp88 residues). The H_2O_2 tolerance of *rDca*UPO-A161C was preliminarily explored by comparing its structure with the wild type. Notably, *rDca*UPO-A161C showed significantly higher catalytic efficiency than the wild type for the production of hydroxyl fatty acids. This study is anticipated to provide an insight into the structure-function relationship and expand potential applications of UPOs.

Unspecific peroxygenases (UPOs, EC 1.11.2.1) is a kind of highly glycosylated thioheme enzyme, which belongs to the heme sulfate peroxygenase (HTP) superfamily [1]. At present, it is documented that UPOs mainly exist in Dikarya, Ascomycota, and Basidiomycota. Under mild conditions, UPOs are capable of catalyzing a variety of oxidations of inert C–H bonds with hydrogen peroxide (H_2O_2) as the only oxygen donor [2], such as hydroxylation [3], epoxidation of compounds containing C=C bonds [4], and sulfide sulfonation [5]. Therefore, UPOs are well-recognized as a potential enzyme for the oxidative functionalization of a wide range of substrates [6] in the fields of food processing [7], pharmaceutical production [8], and environmental protection [9].

Among the types of reactions that UPOs can catalyze, the reaction that catalyzes the hydroxylation of C–H bonds of fatty acids to generate hydroxyl fatty acids is of great significance. Hydroxy fatty acids are saturated or unsaturated fatty acids containing single or multiple hydroxyl groups [10,11]. They have shown great potential in the synthesis of precursors of polyester fiber and polyamides [12,13], lactone and other flavor compounds [14], drug intermediates [15,16], surfactants, and emulsifiers [17]. Due to the limitations and drawbacks of traditional chemical synthesis, the synthesis of hydroxyl fatty acids *via* an enzymatic way has become a research hotspot in recent years [18]. And some UPOs have been successfully used in the synthesis of hydroxyl fatty acids [19–22].

It has been sufficiently demonstrated that UPOs are cofactor-independent enzymes catalyzing oxidative reactions with H_2O_2 as an oxygen donor. However, unfortunately, the formation of iron peroxide in high concentrations of H_2O_2 usually leads to collapsed active heme centers of UPOs due to their strong affinity for H_2O_2 [23]. The poor H_2O_2 tolerance of UPOs has become a bottleneck for their large-scale industrious applications. The combination of a sensitive H_2O_2 sensor and an automatical H_2O_2 feeding system has ever been proposed to solve this issue [24], but the development of this equipment requires unacceptable high costs. To maintain the stability and catalytic activity of UPOs, some *in situ* H_2O_2 generating methods have been established *via* photochemistry [25–28], electrochemistry [29–33], and multi-enzyme cascade [34–37]. High costs and complicated operations are also involved in these approaches, thereby hindering the further applications of UPOs. Despite the impressive advances in the H_2O_2 tolerance research of UPOs in the last department, it scenes that we have merely scratched the surface that far, instead of solving the problem from

* Corresponding authors.
E-mail addresses: myj605740779@scut.edu.cn (Y. Ma), yonghw@scut.edu.cn (Y. Wang).

https://doi.org/10.1016/j.cclet.2023.108701
1001-8417/

the protein structure level. Therefore, clarification of the relationship between structure and H_2O_2 tolerance of UPOs appears to be a potential way for the development of H_2O_2-resistant UPOs based on the molecular modification.

The key to exploring the amino acid sites that affect H_2O_2 tolerance in UPO structure is to obtain protein crystals. Therefore, achieving heterologous expression of UPO and obtaining high-quality enzymes is a prerequisite for protein crystal preparation and analysis. But the heterologous expression of UPOs still faces challenges, since the discovery of the first UPO (*Aae*UPO) in 2004, only about 20 kinds of UPOs have been identified and achieved heterologous expression [38], and just a few protein crystal structures of UPOs have been resolved, including *Aae*UPO (pdb_2YOR) (UPO from *Agrocybe aegerita*) [39], the PaDa-I mutant of *Aae*UPO (pdb_5OXU) [40], *Mro*UPO (pdb_5FUK) (UPO from *Marasmius rotula*), *Hsp*UPO (pdb_7O1R) (UPO from *Hypoxylon* sp. EC38) [41] and *rCvi*UPO (pdb_7ZCL) (UPO from *Collariella virescens*) [42]. Nevertheless, the relationship between structure and H_2O_2 tolerance of UPOs has been hardly elucidated due to the lack of crystal structure of more UPO proteins. Therefore, the rule-of-thumb for the H_2O_2 tolerance-oriented molecular modification of UPOs is still lacking.

To (partially) address this gap, we chose the UPO from *Daldinia caldariorum* (*rDca*UPO) for expression and further investigate the relationship between protein structure and H_2O_2 tolerance in the present study. *rDca*UPO is the second active recombinant UPOs heterologously expressed in *E. coli* and has great potential in catalyzing the hydroxylation reaction of fatty acids [43]. The molecular modification of *rDca*UPO is feasible due to its remarkably higher production level than *Mro*UPO using the same expression system [44]. In this study, we heterologously expressed the *rDca*UPO in the *E. coli* prokaryotic system. We analyzed the amino acid composition near the active center of *rDca*UPO and identified three crucial sites that might affect its H_2O_2 tolerance. Nine mutants were designed to elucidate the relationship between these sites and H_2O_2 tolerance. Gratifyingly, we show that the mutant *rDca*UPO-A161C, exhibited significantly improved H_2O_2 tolerance and higher catalytic efficiency for the enzymatic production of hydroxyl fatty acids compared with the wild type. The mechanism for H_2O_2-tolerance improvement of *rDca*UPO-A161C was preliminarily analyzed based on its crystal structure. This study would provide an insight into the relationship between structure and H_2O_2 tolerance of UPOs.

Compared with the "short" UPOs with reported structures, the protein sequence similarity between *rDca*UPO and *Hsp*UPO is as high as 67% (Fig. 1 and Table S1 in Supporting information). The phylogenetic analysis of *rDca*UPO showed that *rDca*UPO was clustered together with *Hsp*UPO in the phylogenetic tree, suggesting that *rDca*UPO might have the same functional properties (Fig. S1 in Supporting information). This observation also provided a theoretical basis for the subsequent template selection for *rDca*UPO homologous modeling.

The *rDca*UPO wild type and its mutants were expressed in *E. coli* BL21 (DE3). The crude enzyme solution was eluted by a Ni affinity chromatography column and the purity of desalted enzyme solution met the requirements of subsequent experiments (Fig. S2 in Supporting information). The biochemical properties of *rDca*UPO were determined by the NBD method (Table S2 and Fig. S3 in Supporting information). The optimum temperature of *rDca*UPO was 30 °C and the optimum pH was 6, suggesting the stability in a neutral and partial acid environment. Metal ions Fe^{3+} and Fe^{2+} promoted the enzyme activity of *rDca*UPO, and *rDca*UPO was not sensitive to most organic solvents and metal ions.

Usually, each UPO-catalyzed reaction requires two H_2O_2 molecules. Karich *et al.* found that the decomposition process of the second H_2O_2 is similar to the peroxidase reaction of UPOs [45].

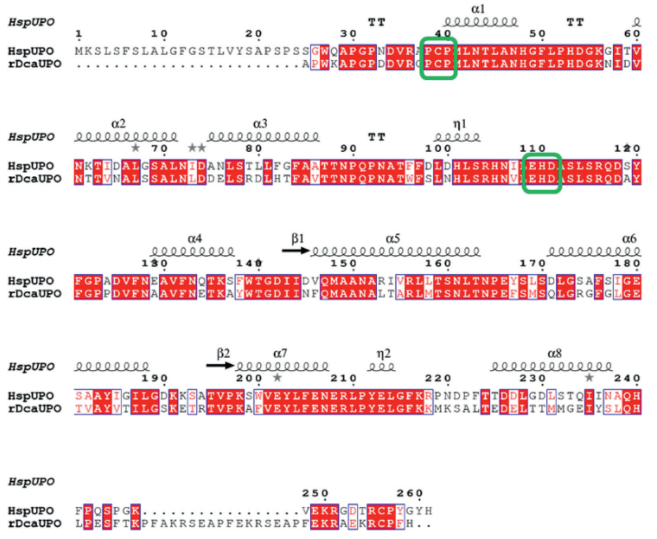

Fig. 1. Structure-based amino acid sequence alignment of the mature *rDca*UPO with the template *Hsp*UPO. Residues in the conserved PCP and EHD motif of the UPOs family were green frames.

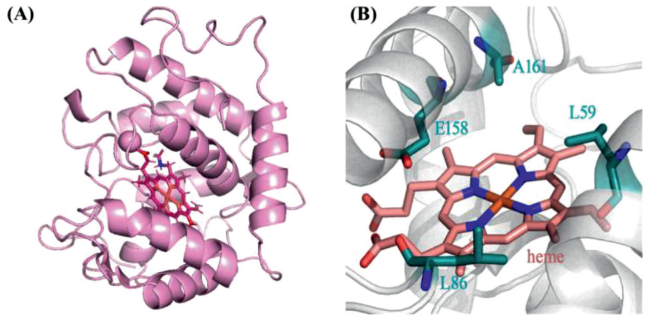

Fig. 2. Selection of amino acid key sites in the region near the active center (green) of *rDca*UPO. (A) The overall structure of the *rDca*UPO wild type. (B) Amino acid key sites of the active center of the *rDca*UPO wild type.

Cpd-I extracts a hydrogen atom from the second H_2O_2 to form Cpd-II. In heme-dependent catalase, distal histidine (His56) or asparagine (Asn129) stabilizes the H_2O_2 free radical ($HOO^{\bullet}$) through hydrogen bonding. The excess H_2O_2 will lead to the formation of Cpd-III (iron superoxide complex = [Fe^{III}-O^{2-}]). When Cpd-III encounters extra H_2O_2, the formed hydroxyl radical ($HO^{\bullet}$) will eventually induce the following formation of biliverdin *via* the "self-hydroxylation" of heme, thereby inactivating UPOs [45].

Therefore, to protect the active "heme" center from excess H_2O_2 molecules and decelerate the heme "bleaching" by formed $HO^{\bullet}$, some reductive amino acids were introduced near the catalytic center of the wild type *rDca*UPO (Fig. 2A). Based on the redox properties of amino acids near the catalytic active center in the tertiary structure of *rDca*UPO, the mutation targets were selected and replaced with some reduced amino acids (Fig. 2B). The *rDca*UPO mutants include L59R, L59S, L59C, L86F, L86R, A161R, A161S, A161C, and A161K.

To detect the effect of mutants on heme protection, firstly, the optimal H_2O_2 concentration of the *rDca*UPO wild type and mutants were compared using NBD as substrate. As shown in Fig. 3A, the *rDca*UPO wild type and mutants L59R, L86F, A161R, A161S, and A161C showed an optimum H_2O_2 concentration of 10 mmol/L, whereas the optimum H_2O_2 concentration of A161K decreased to 5 mmol/L. Therefore, mutations of these key amino acids changed the optimal H_2O_2 concentration of *rDca*UPO.

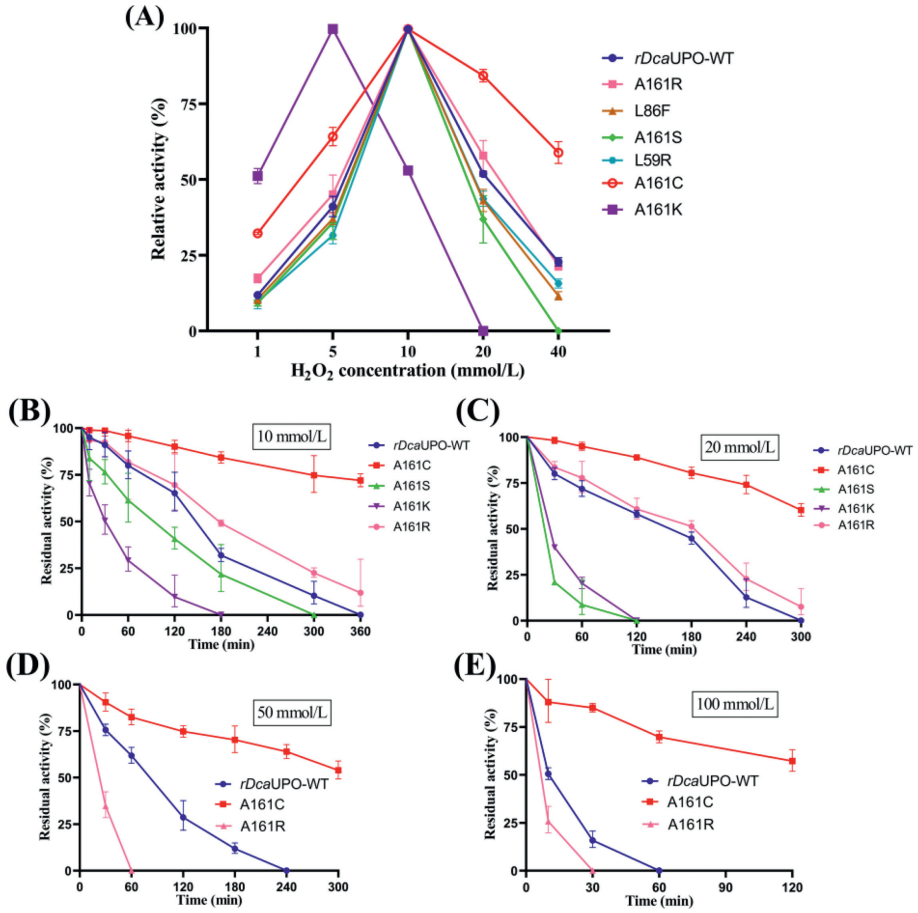

Fig. 3. The optimal H_2O_2 concentrations and H_2O_2 stability of the *rDca*UPO wild type and mutants. (A) Optimal H_2O_2 concentration. (B) The H_2O_2 stability under 10 mmol/L H_2O_2. (C) The H_2O_2 stability under 20 mmol/L H_2O_2. (D) The H_2O_2 stability under 50 mmol/L H_2O_2. (E) The H_2O_2 stability under 100 mmol/L H_2O_2. Values were means ± standard deviation from three independent experiments.

The H_2O_2 tolerance of the *rDca*UPO wild type and mutants was further studied at different H_2O_2 concentrations. As shown in Figs. 3B–E and Table S3 in Supporting information, the H_2O_2 tolerance of these mutants changed compared with the wild type under different H_2O_2 concentrations (10, 20, 50, and 100 mmol/L). The residual enzyme activities of L59R, L86F, and A161K could not be detected after incubation with 10 mmol/L H_2O_2 for 4 h. The *rDca*UPO mutants with mutations at A161 using amino acids of increased reducibility exhibited increased H_2O_2-tolerance. Compared with the wild type, the relative enzyme activity of A161K was 117%. Notably, the mutant *rDca*UPO-A161C showed a higher H_2O_2 tolerance compared with other mutants. After incubation in 10 mmol/L H_2O_2, the half-life of enzyme activity was increased from 2.5 h to 12.5 h. After incubation in a high concentration of H_2O_2 (100 mmol/L), the half-life of enzyme activity was still more than 2 h, and the relative enzyme activity increased by 64%. The introduction of reductive amino acids near the active center of *rDca*UPO contributed greatly to improved H_2O_2 tolerance.

To further mechanistically explain the improved H_2O_2 tolerance of *rDca*UPO-A161C, the crystal of *rDca*UPO-A161C was prepared for structural analysis (Fig. S4 in Supporting information). The crystal structure of the ligand-free *rDca*UPO-A161C was obtained at 1.47 Å resolution by the molecular replacement (MR) method. The data collection and refinement statistics are shown in Table S4 (Supporting information). The three-dimensional structure of *rDca*UPO-A161C was uploaded to the PDB database (pdb_8IAG). The overall structure of *rDca*UPO-A161C monomers (Fig. 4A) is compact and spherical. It consists of residues from Ala1 to Thr224, displaying

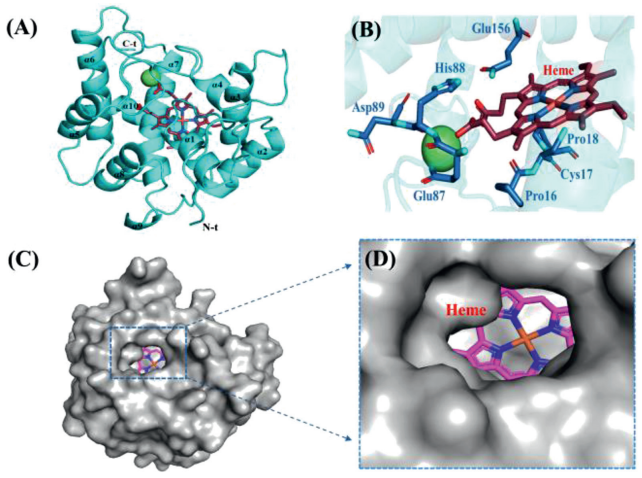

Fig. 4. Structures of mutant *rDca*UPO-A161C. (A) The overall structure of the mutant *rDca*UPO-A161C. (B) Active sites of the mutant *rDca*UPO-A161C. (C) Surface display of the mutant *rDca*UPO-A161C. (D) Pocket of the mutant *rDca*UPO-A161C.

clearly defined electron density together with one heme molecule (CPK sticks with Fe^{3+} as a red stick) and one Mg^{2+} ion (green sphere). The overall fold of *rDca*UPO-A161C mutant contains a total of 10 α-helixes (cyan) and a series of ordered rings, the combination of which form a single asymmetric spherical structure. α-Helices include two short α4 and α9 helices (L77-S81 and Y90-

L92) (Fig. 4A). Moreover, the two conserved domains near heme form an active site with the catalytic PCP regions (Pro16, Cys17, Pro18 residues) and EHD regions (Glu86, His87, Asp88 residues) (Fig. 4B). The heme co-factor is embedded within helices with the thiolate sulfur of Cys-17 coordinating with the heme iron. This pattern is attributed to the highly conserved "Peroxidase_2" domain (National Center for Biotechnology Information (NCBI) blastp) of chloroperoxidases [46,47]. Figs. 4C and D showed the surface pattern of the overall structure of *rDca*UPO-A161C. The shape of the distal matrix binding bag is similar to the truncated cone. The entry channel directly contacts the Fe^{3+} ion above the distal heme.

The structural characterization showed that *rDca*UPO-A161C has a similar three-dimensional structure to two "short" UPOs, *i.e.* *Hsp*UPO and *rCvi*UPO (Fig. 5A), with α helix being the primary structure. The structural difference is that *Hsp*UPO contains two β-sheets (I143-D145 and T195-P197). Similarly, the α-helix includes two short α4 (P72-K74) and α6 (Y99-H102) of *rCvi*UPO, which were not found in *rDca*UPO-A161. The structural superposition showed that the active regions of PCP and EHD are highly conserved in the "short UPO family". In *rDca*UPO-A161C, in addition to the conserved amino acids of the active site, the heme pocket includes residues arranged on the inside of the cavity, such as Leu86, Met19, Leu59, Cys161, and Glu158 (Fig. 5B). Mg^{2+} ion seem to be coordinated by His87 (backbone) carbonyl, two water molecules, carboxyl groups of Glu86, and a heme ring. In this structure, Mg^{2+} ion appear to anchor the heme cofactor in the central pocket of UPOs. In the same spatial position of *Hsp*UPO (Fig. 5C), the amino acid residues around the heme pocket are the same as those of *rDca*UPO-A161C, which is consistent with the amino acid sequence similarity (67%) of these two proteins. In the heme pocket of *rCvi*UPO, consistent with *rDca*UPO-A161C, the heme iron is coordinated by the mercaptan side chain of Cys19 towards the lower side (Fig. 5D). The differences between the residues around the cofactor *rDca*UPO (cyan) and *rCvi*UPO (yellow) are that the equivalent positions of Leu86, Leu59, and Met19 in *rDca*UPO-A161C become Phe88, Ile61, and Ala21 in *rCvi*UPO, thus reducing the entrance to the channel.

The structure of *rDca*UPO-A161C was regarded as a template to reconstruct the three-dimensional structure of the *rDca*UPO wild type. To explore the improvement of H_2O_2 tolerance by *rDca*UPO-A161C, the structure of *rDca*UPO-A161C was compared with the *rDca*UPO wild type (Fig. 5E). The conserved regions of PCP and EHD

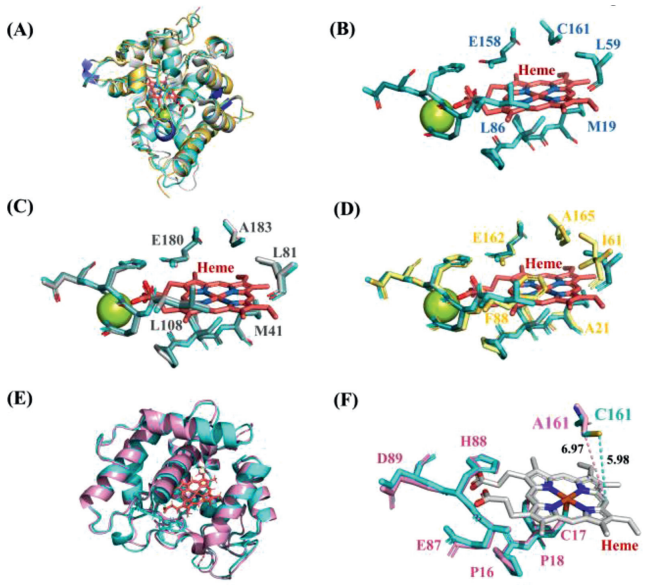

Fig. 5. Stereo-view of the superimposition and the comparison of heme pocket residues (top) and access channels (bottom) between mutant *rDca*UPO-A161C and other UPOs. (A) The overall structure comparison. (B) Active site key amino acids of mutant *rDca*UPO-A161C. (C) The active site differences between mutant *rDca*UPO-A161C (cyan) and *Hsp*UPO (gray). (D) The active site differences between mutant *rDca*UPO-A161C (cyan) and *rCvi*UPO (yellow). (E) Superposition of mutant *rDca*UPO-A161C and wild type overall structure. (F) Major differences between mutant *rDca*UPO-A161C and wild type (mutant in blue, wild type in pink).

are located around an exposed heme in the catalytic center of the mutant (Fig. 5F). The results showed that the positions of heme in its active center and crucial amino acids including P16, C17, P18, and E87, H88, and D89 contributed to the unchanged catalytic oxidation function.

The active site of UPOs is a conical closed channel. Cys acts as a heme ligand coordinated by the sulfhydryl side chain to stabilize the entire active site [26]. The Cys17 was used as the ligand for stabilizing the heme pocket of *rDca*UPO-A161C in this study. The introduction of Cys near the upper pocket of the heme, to some extent, seemed to increase the stability of the heme pocket.

Table 1
The catalytic reaction of *rDca*UPO and *rDca*UPO-A161C on fatty acid substrates with different chain length.

Substrate	Product	Concentration (mmol/L)
Octanoic acid	$\omega-1$ octanoic acid	WT, 0.02; A161C, 0.07
Nonanoic acid	$\omega-1$ nonanoic acid	WT, 0.05; A161C, 0.12
Decanoic acid	$\omega-1$ decanoic acid	WT, 0.12; A161C, 0.20
Undecanoic acid	$\omega-1$ undecanoic acid	WT, 0.20; A161C, 0.28
Lauric acid	$\omega-1$ lauric acid	WT, 0.22; A161C, 0.38

Reaction conditions: $[H_2O_2]=2$ mmol/L, [UPO] = 0.5 U, [fatty acid substrate] = 1 mmol/L, [buffer] = 50 mmol/L phosphate buffered saline (PBS), pH 7.0, 30 °C, 500 rpm, 12 h. The identification and analysis of the product were determined by gas chromatography-mass spectrometry (GC–MS). See Supporting information for the detailed gas chromatogram and mass spectrogram (Figs. S5–S9).

Further structural analysis showed that the distance between the SH motif of the mutant Cys at position 161 and the C atom of the hydroxylation site on heme is 5.98 Å. In comparison, the distance of the C atom of the *rDca*UPO wild type Ala is 6.97 Å (Fig. 5F). The -SH motif of the Cys of *rDca*UPO-A161C is closer to the oxidation site above the heme than Ala of the wild type. It is speculated that the 161C position of *rDca*UPO-A161C would be the initial reaction site when exposed to excessive hydroxyl radicals, thus delaying the bleaching process of heme. As a result, the inactivation process of *rDca*UPO-A161C would be indirectly slowed down. This assumption is in agreement with the observation that *rDca*UPO-A161C showed robust H_2O_2-tolerance.

The catalytic oxidations of C8-C12 saturated straight-chain fatty acids by *rDca*UPO and *rDca*UPO-A161C were investigated. As shown in Table 1, *rDca*UPO and *rDca*UPO-A161C showed high hydroxylation reaction efficiency on the $\omega-1$ position of C8-C12 fatty acids. Both *rDca*UPO and *rDca*UPO-A161C preferred to catalyze the hydroxylation of lauric acid. The concentration of $\omega-1$ hydroxylated lauric acid produced by *rDca*UPO-A161C was 0.38 mmol/L, which was higher than that of the wild-type.

In conclusion, we reported a structure-guided enzyme engineering approach for improving the H_2O_2-tolerance of UPOs. Using this approach, we designed a mutant, *i.e., rDca*UPO-A161C, which exhibited significantly enhanced H_2O_2-tolerance, enabling the hydroxylation of C8-C12 saturated straight-chain fatty acids. The structure-H_2O_2-tolerance relationship reported in this study would provide an insight into the design of function-targeted UPOs by structure-guided engineering.

Declaration of competing interest

The authors declare that they have no known competing financial interests or personal relationship that could have appeared to influence the work reported in this paper. Guangdong Youmei Institute of Intelligent Bio-manufacturing Co., Ltd. provides some experimental instruments for testing during the whole experiment process. The company will not have any conflict of interest.

Acknowledgments

This work was supported by the National Natural Science Foundation of China (No. 32001633), the Key Program of Natural Science Foundation of China (No. 31930084), and Guangzhou Science and technology planning project (No. 202102020370).

Supplementary materials

Supplementary material associated with this article can be found, in the online version, at doi:10.1016/j.cclet.2023.108701.

References

[1] M. Hofrichter, R. Ullrich, Appl. Microbiol. Biotechnol. 71 (2006) 276–288.
[2] M. Faiza, S.F. Huang, D.M. Lan, Y.H. Wang, BMC Evol. Biol. 19 (2019) 76.
[3] D.H. Anh, R. Ullrich, D. Benndorf, et al., Appl. Environ. Microbiol. 73 (2007) 5477–5485.
[4] C. Aranda, R. Ullrich, J. Kiebist, et al., Catal. Sci. Technol. 8 (2018) 2394–2401.
[5] I. Bassanini, E.E. Ferrandi, M. Vanoni, et al., Eur. J. Org. Chem. 2017 (2017) 7186–7189.
[6] C. Yun, J. Kim, F. Hollmann, C.B. Park, Chem. Sci. 13 (2022) 12260.
[7] E. Fernandez-Fueyo, Y. Ni, A.G. Baraibar, et al., J. Mol. Catal. B 134 (2016) 347–352.
[8] P.G. De Santos, M. Canellas, F. Tieves, et al., ACS Catal. 8 (2018) 4789–4799.
[9] A. Karich, R. Ullrich, K. Scheibner, M. Hofrichter, Front. Microbiol. 8 (2017) 1463.
[10] Y. Cao, X. Zhang, Appl. Microbiol. Biotechnol. 97 (2013) 3323–3331.
[11] N.N. Farshori, M.R. Banday, Z. Zahoor, A. Rauf, Chin. Chem. Lett. 21 (2010) 646–650.
[12] C.T. Hou, R.J.F. Forman, J. Ind. Microbiol. Biotechnol. 24 (2000) 275–276.
[13] S.Y. Shin, H.R. Kim, S.C. Kang, J. Biol. Chem. 47 (2004) 205–208.
[14] J. Trzaskowski, D. Quinzler, C. Bahrle, et al., Macromol. Rapid Comm. 32 (2011) 1352–1356.
[15] P.M. Chaudhari, P.V. Kawade, S.M. Funne, Int. J. Pharm. Technol. 3 (2011) 774–798.
[16] M.R. Banday, A. Rauf, Chin. Chem. Lett. 19 (2008) 1427–1430.
[17] G.F. Koay, T.G. Chuah, S. Zainal-Abidin, J. Oleo Sci. 60 (2011) 237–265.
[18] X.P. Duan, J.Q. Gao, Y.J.J. Zhou, Chin. Chem. Lett. 29 (2018) 681–686.
[19] M. Municoy, A. González-Benjumea, J. Carro, et al., ACS Catal. 10 (2020) 13584–13595.
[20] T.T. Li, H.J. Liang, B. Wu, et al., Mol. Catal. 546 (2023) 113275.
[21] O. Andres dR, C. Jose, K. Jan, et al., Chem. Eur. J. 23 (2017) 16985–16989.
[22] A. Gonzalez-Benjumea, J. Carro, C. Renau-Minguez, et al., Catal. Sci. Technol. 10 (2020) 717–725.
[23] K. Alina, R. Katrin, L. Stephan, Front. Bioeng. Biotech. 9 (2021) 705630.
[24] S. Bormann, A. Gomez Baraibar, Y. Ni, et al., Catal. Sci. Technol. 5 (2015) 2038.
[25] W.Y. Zhang, E. Fernandez-Fueyo, Y. Ni, et al., Nat. Catal. 1 (2018) 55–62.
[26] S.J.P. Willot, E. Fernandez-Fueyo, F. Tieves, et al., ACS Catal. 9 (2019) 890–894.
[27] B. Yuan, D. Mahor, Q. Fei, et al., ACS Catal. 10 (2020) 8277–8284.
[28] H.L. Wapshott-Stehli, A.M. Grunden, Enzyme Microb. Tech. 145 (2021) 109744.
[29] D. Holtmann, T. Krieg, L. Getrey, J. Schrader, Catal. Commun. 51 (2014) 82–85.
[30] N. Guillet, L. Roue, S. Marcotte, et al., J. Appl. Electrochem. 36 (2006) 863–870.
[31] G. Gideon, JACS Au 1 (2021) 1312–1329.
[32] D.S. Choi, Y. Ni, E. Fernandez-Fue, et al., ACS Catal. 7 (2017) 1563–1567.
[33] S. Bormann, M.M.C.H. van Schie, T.P. De Almeida, et al., ChemSusChem 12 (2019) 4759–4763.
[34] L.T. Nguyen, K.L. Yang, Enzyme Microb. Tech. 100 (2017) 52–59.
[35] Y. Ni, E. Fernandez-Fueyo, A.G. Baraibar, et al., Angew. Chem. Int. Ed. 55 (2016) 798–801.
[36] F. Tieves, S.J.P. Willot, M.M.C.H. van Schie, et al., Angew. Chem. Int. Ed. 58 (2019) 7873–7877.
[37] M.M.C.H. Van Schie, J.D. Sporing, M. Bocola, et al., Green Chem. 23 (2021) 3191–3206.
[38] M.Y. Lai, J. Wei, J.H. Xu, et al., Synth. Biol. J. 3 (2022) 1235–1249.
[39] K. Piontek, E. Strittmatter, R. Ullrich, et al., J. Biol. Chem. 288 (2013) 34767–34776.
[40] M. Ramirez-Escudero, P. Molina-Espeja, P. Gomez De Santos, et al., ACS Chem. Biol. 13 (2018) 3259–3268.
[41] L. Rotilio, A. Swoboda, K. Ebner, et al., ACS Catal. 11 (2021) 11511–11525.
[42] D. Linde, E. Santillana, E. Fernández-Fueyo, et al., Antioxidants 11 (2022) 891.
[43] D. Linde, A. Olmedo, A. González-Benjumea, et al., Appl. Environ. Microbiol. 86 (2020) 2899–2919.
[44] M. Hofrichter, H. Kellner, R. Herzog, et al., Antioxidants 11 (2022) 163.
[45] K. Alexander, C. Katrin, U. Rene, et al., J. Mol. Catal. B 134 (2016) 238–246.
[46] M. Sundaramoorthy, J. Terner, T.L. Poulos, Structure 3 (1995) 1367–1377.
[47] M.J. Pecyna, R. Ullrich, B. Bittner, et al., Appl. Microbiol. Biotechnol. 84 (2009) 885–897.